A practical macromechanical-based model for the bend capacity of FRP bars

Author 1

- Thanongsak Imjai, BEng, MSc, PhD
- School of Engineering and Technology, Walailak University, Nakhonsithammarat, Thailand

Author 2

- Maurizio Guadagnini, MEng, PhD
- Dept. of Civil and Structural Engineering, The University of Sheffield, Sheffield, UK

Author 3

- Kypros Pilakoutas, MEng, MSc, PhD, DSc, ACGI, DIC
- Dept. of Civil and Structural Engineering, The University of Sheffield, Sheffield, UK.

Author 4

- Reyes Garcia, MEng, MSc, PhD
- School of Engineering, The University of Warwick, Coventry, UK.

Author 5

- Piti Sukontasukkul, MEng, MSc, PhD
- Dept. of Civil Engineering, King Mongkut University of Technology North Bangkok, Thailand

Author 6

- Suchart Limkatanyu, MEng, MSc, PhD
- Dept. of Civil Engineering, Prince of Songkla University, Hadyai, Songkhla, Thailand

Corresponding author: thanongsak.im@wu.ac.th

Abstract. Bent Fibre Reinforced Polymer (FRP) bars embedded in reinforced concrete elements resist lower forces than straight counterparts due to strength losses at the bend, and such losses are difficult to calculate. This article investigates the effect of section geometry and bond and proposes a new macromechanical-based model to calculate the bend capacity of FRP bars. The proposed model uses a Tsai-Hill failure criterion and accounts for factors known to influence the bend capacity of FRP bars. A section factor (ignored in existing models) also accounts for the strength degradation due to the change in geometry at the bent portion of the FRP bar. The model is calibrated using a set of 80 tests found in the literature and performed by the authors. The results indicate that, compared to existing equations, the proposed model predicts the bend strength of FRP bars more accurately (average Prediction/Experiment ratio of 1.0 and standard deviation of 0.25). Following validation and verification, appropriate values for the model parameters are recommended for design. The proposed model can lead to more economic design (by up to 15%).

*Keywords***:** Buildings, structures & design; Composite structures; Strength & testing of materials; Concrete Structures; FRP

1. Introduction

Fibre Reinforced Polymer (FRP) bars are often used as internal reinforcement in concrete structures exposed to aggressive or wet environments. In general, the use of FRP bars is expected to i) increase the durability of the structure and ii) reduce future maintenance and repair costs, which can be much higher than the initial construction costs of the structure (Pilakoutas et al. 2011; Imjai et al. 2016; Stuart and Cunningham 2017). Typically, the internal reinforcement in concrete structures is not continuous, and therefore bars have to be bent (curved or shaped) at some point in the elements. The reason for the slow uptake of FRPs as internal reinforcement can be partly due to the lack of commercially available curved/shaped bars that can be used as shear links or reinforcement in complex beam-column connections. Moreover, FRP profiles are not produced to a regular standard as opposed to commercial steel bars.

The majority of the reinforcing bars currently used in construction of concrete structures consist of steel bars, which are pre-bent before being delivered to the site. Existing guidelines for cold bending of (mild) steel bars specify a bending radius to bar diameter ratio of 2 (BSI 2000), which results in a plastic strain of 20% in the extreme fibre of a bar (see Figure 1). However, the typical ultimate longitudinal strain value of curved FRP products varies from 1% to 2.5%, and therefore the strain induced in the fibres due to bending/curving has to be carefully controlled to prevent premature failures. As a result, cold bending of FRP bars requires much larger bending radius to bar diameter ratios than those used for steel reinforcement, as shown in Figure 1 (Imjai et al. 2009). In the case of shear links, preformed curved FRP bars with much smaller radii are often necessary. While steel bars can be bent without any loss of strength, previous research has indicated that the tensile strength of FRP rods can reduce by up to 60% under a combination of tensile and shear stresses (Ahmed et al. 2010; Ishihara et al. 1997; Lee et al. 2014; Maruyama et al. 1993; Shehata et al. 2000). Past research indicates that the reduction in capacity depends on factors such as the radius of the bend, bond properties and type of anchorage provided (Ehsani et al. 1995; Imjai et al. 2016; Shehata et al. 2000; Ueda et al. 1995).

Other factors that can reduce the bend capacity of FRP bars are related to the materials and techniques used in their manufacturing. For instance, FRP bars are normally produced by pultrusion using thermoset resins. Once the resin is fully set, FRP bars cannot bend easily. Different techniques were examined in the past to produce bent shapes such as 1) resin-impregnated fibres wound onto mandrels to produce closed shapes (e.g. shear links); 2) use of thermoset resins where bents are made by partial curing of resins during pultrusion, and subsequent bending of the bar prior to full setting; and 3) use of thermoplastic resins where the fully set bar can be warmed up and bent to shape. Whilst method 1 can produce good consistent bent sections, methods 2 and 3 usually 'flattens' the bent cross-section, which in turn induces fibre buckling on the inner face of the bent bar, thus reducing the bar capacity further (Ahmed et al. 2010; Imjai et al. 2017).

Limited research has investigated the effect of bends on the strength of FRP stirrups. Nakamura and Higai (1995) conducted a theoretical study on the bend capacity of FRP stirrups using tests results from Miyata et al. (1989). Nakamura and Higai assessed the variation of the tensile strength of bent FRP rods pulled in tension by considering bending radius of 10, 15, 20, 25, and 30 mm. The 10 mm hybrid FRP rods were made of glass and carbon fibres impregnated with resin, which were in turn embedded in a 200x400 concrete block. Based on the results, Nakamura and Higai proposed Equation 1 to calculate the strength of bent FRP bars:

$$\frac{\sigma_b}{\sigma_{1max}} = \frac{r}{d} ln\left(1 + \frac{d}{r}\right)$$

(1)

where σ_b is the ultimate strength of the bend, σ_{1max} is the ultimate strength parallel to the FRP fibres, r is the bend radius, and d is the nominal bar diameter.

Ishihara et al. (1997) carried out 2D finite element analysis to examine the behaviour of bent FRP stirrups embedded in concrete using the test data by Ueda et al. (1995). The analytical results showed that the strength of a bar at its bent portion increases with the bending radius. Based on a parametric study and a limited data, Ishihara et al. proposed an empirical expression (Equation 2) to calculate the strength of bent FRP bars:

$$\frac{\sigma_b}{\sigma_{1max}} = \frac{1}{\lambda}ln(1 + \lambda) \qquad (2)$$

where $ln\lambda = 0.90 + 0.73ln\,(d/r)$, and the rest of the variables are as defined before.

It should be noted that Equation 2 is similar to Equation 1 but with *λ=d/r*. While Ishihara et al. study showed that the reduction in strength depended heavily on the type of FRP, more recent experimental evidence confirmed that the bond properties and differential slippage of the FRP bar can also affect the strength reduction (Imjai et al. 2017), both of which are neglected in Equations 1 and 2 as limited research existed on the subject.

The Japan Society of Civil Engineers (JSCE) guidelines (JSCE 1997) propose to calculate σ_b using Equation 3:

$$\sigma_b = (\alpha \frac{r}{d} + 0.3)\sigma_{1max} \leq \sigma_{1max} \qquad (3)$$

where the factor *α*=0.05 corresponds to a 95% confidence limit, and *α*=0.092 corresponds to a 50% confidence limit.

More recently, Lee et al. (2014) modified Equation 3 to account for bars of non-circular section. Accordingly, they suggested converting non-circular bars to equivalent circular bars, and then use Equation 4 in the calculations:

$$\sigma_b = 0.02(\alpha \frac{r}{d_{fi}} + 0.47)\sigma_{1max} \leq \sigma_{1max} \qquad (4)$$

where d_{fi} is the diameter of the equivalent circular section that can be approximated as a function of the bar thickness. Lee et al. also proposed different values of *α* (suitable for Equation 3) using linear regression analysis from 14 tests.

It should be noted that Equations 3 and 4 are empirical and only depend on the geometry of the bend, whilst the type of FRP is neglected. Recent research by the authors (Imjai et al. 2017) has demonstrated that the prediction of these models are inconsistent with the experimental data

available in the literature. As a result, there is a need to develop more reliable and practical models to predict the capacity of bent FRP reinforcement.

This article proposes a new and practical macromechanical model to calculate the strength of bent FRP bars. The proposed model accounts for the geometry of the bend, as well as for the type of material and properties of the bar. The proposed model is validated using an extensive experimental dataset available in the literature, and tests performed by the authors. This article contributes towards developing practical design equations suitable for incorporation into future FRP guidelines for concrete structures.

2. Proposed macromechanical-based failure model

2.1. Stress distribution along bent reinforcement

If a bent bar embedded in concrete is subjected to internal forces, the distribution of internal stresses along the bar would depend on the geometry of the bar and on the bond properties between concrete and bar. For instance, a corner of a shear stirrup will have average stresses acting on the bent portion of the link (ignoring bond stresses) as shown in Figure 2a. For simplicity, it can be assumed that the concrete applies uniform (equivalent hydrostatic) pressure along the bent portion of the stirrup. Force equilibrium of the rigid body (see Figure 2a) along the horizontal and vertical directions would be defined by Equation 5:

$$\sigma_1 . t . b = \sigma_2 . r . b \tag{5}$$

Or in a simplified form:

$$\sigma_2 = \frac{\sigma_1 . t}{r} \tag{6}$$

In Equations 5 and 6, σ_1 is the tensile stress developed in a straight bar, σ_2 is the compressive stress applied by the confined concrete perpendicular to the fibres, r is the internal bending radius, and b and t are the width and the thickness of the bar, respectively. It should be noted that, since the above equations neglect the bond between concrete and reinforcement, the

predicted bend strength given by the equations will be more conservative (e.g. in the case a crack propagates through the bent corner of the FRP stirrup).

2.2. *Failure criteria for unidirectional composites*

Figure 2a shows that σ_1 and σ_2 create a biaxial state of stress on the bent portion of the FRP bar. For composite materials, such state of stresses can be solved using the Tsai-Hill failure criteria (Tsai and Hahn 1980). Accordingly, for a plane stress in the 1-2 plane (i.e. for $\sigma_3 = \tau_{13} = \tau_{23} = 0$) of a transversely isotropic material, the failure surface is defined by:

$$\frac{\sigma_1^2}{\sigma_{1max}^2} - \frac{\sigma_1\sigma_2}{\sigma_{1max}^2} + \frac{\sigma_2^2}{\sigma_{2max}^2} + \frac{\tau_{12}^2}{\tau_{max}^2} = 1 \tag{7}$$

where σ_{1max} is the longitudinal tensile strength, σ_{2max} is the transversal tensile strength, and τ_{max} is the in-plane shear strength.

By substituting Equations 5 and 6 into Equation 7 for the case illustrated in Figure 2a and rearranging terms, Equation 8 can be used to define the ratio between the maximum stress resisted along the bend of the composites σ_1, and its unidirectional tensile strength σ_{1max}:

$$\frac{\sigma_1}{\sigma_{1max}} = \frac{\sqrt{1-\varphi^2}}{\sqrt{1+\left(\frac{t}{r}\right)+\left(\frac{t}{r}\right)^2 \beta^2}} \tag{8}$$

where $\varphi = \tau_{12}/\tau_{max}$, and $\beta = \sigma_{1max}/\sigma_{2max}$.

It should be noted that Equation 8 assumes that the FRP bar has a rectangular cross-section. For a round bar, the factor $\pi d/4$ replaces the bar thickness, *t*, as defined in Equation 9.

$$\frac{\sigma_1}{\sigma_{1max}} = \frac{\sqrt{1-\varphi^2}}{\sqrt{1+\left(\frac{\pi d}{4r}\right)+\left(\frac{\pi d}{4r}\right)^2 \beta^2}} \tag{9}$$

Equations 8 and 9 indicate that the strength of a bent unidirectional FRP bar depends on: 1) the geometry of the bent (*r/t* or *r/d*); 2) the ratio between the shear stress, τ_{12}, and the maximum ratio φ (also referred to as 'bond factor' in subsequent sections of this study); and 3) the ratio of the longitudinal tensile strength and transverse compressive strength of the composite material

β. The influence of these parameters on the bend capacity of FRP bars is examined in the following sections.

2.3. Factors influencing the bend capacity

2.3.1. Effect of 'bond factor' and shear stress correlation

To account for the effect of transverse and shear stresses on the bend capacity of unidirectional composites, the Mohr's brittle fracture criterion can be used. Figure 2b shows that the presence of shear stress, τ_{12}, increases the principal stresses (σ_{1p}, σ_{2p}) in both σ_1 and σ_2. Therefore, for a given set of normal stresses and shear stress (σ_{1p}, σ_{2p}, τ_{12}), the bend capacity can be analysed using the principal stresses based on Tsai-Hill's criterion (Equation 7). Figure 3a shows the bend capacity for different ratios r/d as a function of shear stress (τ_{12}) for an average value of maximum shear strength of typical unidirectional composites used as reinforcement (τ_{max}=40 MPa (Weatherhead 1980; Imjai et al. 2017)). The results show that the bend capacity decreases with an increase of the 'bond factor' φ (i.e. an increase in the value τ_{12}). In general, the magnitude of τ_{max} is much higher than the expected stress in concrete and interlaminar shear failure (within the FRP itself) is unlikely to occur, unless the composite is subjected to high transversal loads. Figure 3b shows the bend capacity of the unidirectional composites as a function of φ. The results shown in this figure were calculated using a value β=7.5, as obtained from tests performed by the authors (Imjai et al. 2017) and described later in section 3.1. The results in Figure 3b indicate that for a bent unidirectional composite subjected to tension (Figure 2), φ tends to be small and usually lower than 0.2. As a result, bond can be neglected when determining the bend capacity of the material (Imjai et al. 2017).

2.3.2. Effect of strength factor

In general, unidirectional composites have higher strength in the direction parallel to the fibres (i.e. σ_{1max} >> σ_{2max}). Also, the longitudinal tensile strength of unidirectional composites can be five or more times higher than the transverse compressive strength (Gibson 1994; Hollaway 1993). Figure 4 shows the effect of β on the bend capacity of the composite. It is shown that the capacity of a bent unidirectional composite increases as β decreases (i.e. with higher values of σ_{2max}). The

results in the figure also confirm that the bend capacity depends heavily on the β value selected for calculations. As such, the selection of an suitable β value to use in the proposed model is not trivial and therefore it is discussed in more detail in section 3.2.

2.3.3. Effect of cross-section geometry

Variations in the geometry of the bent portion of the composite can affect the stress-strain fields along the reinforcement, and thus influence the capacity of the bent portion. In the proposed model, variations in cross-section geometry and fibre orientation are accounted for through a section factor ψ. Figure 5a shows how FRP bars 'kink' at bends during failure, whilst Figure 5b shows how ψ is calculated for circular or rectangular bars. Note that $\psi=1$ in the straight section (i.e. no change in cross-section before and after the bent section), whereas $\psi<1$ in the bend region.

Equation 9 was derived considering that the bar cross section is constant. To account for the actual geometry of the bent portion (for a circular bar), the force equilibrium of the bent portion of the bar can be calculated using:

$$\sigma_2 = \frac{\sigma_1 \pi d}{4r} \cdot \left(\frac{d}{d_b}\right) = \frac{\sigma_1 \pi d}{4r} \cdot \psi \tag{10}$$

where d is the nominal diameter, d_b is the projected diameter at the bent section of a bar, and ψ is the section factor ($\psi=d/d_b \leq 1$).

By multiplying the diameter, d, and the section factor, ψ, Equation 10 can be rewritten as:

$$\frac{\sigma_1}{\sigma_{1max}} = \frac{\sqrt{1-\varphi^2}}{\sqrt{1 + \left(\xi \cdot \frac{\psi}{r}\right) + \left(\xi \cdot \frac{\psi}{r}\right)^2 \beta^2}} \tag{11}$$

where ξ is $\frac{\pi d}{4}$ or t for circular or rectangular cross-sections, respectively.

Figure 6 compares the effect of ψ on the bend capacity of FRP bars according to Equation 11. It is shown that the bend capacity increases as ψ decreases. This is because the radial stresses depend on the geometry at the bent section, which reduce when $d_b>d$ (i.e. $\psi<1$). Also, for a constant radius or r/d, an increase in the bar width (d_b or b_b) at the bent increases the bend

capacity. However, the variation of the cross-section is difficult to measure in practice. Therefore, ψ can be set equal to 1 for the proposed macromechanical model as this leads to a more conservative prediction of the bend capacity of unidirectional composites.

Based on the previous discussion, a bond factor $\varphi=0$ and a shape factor $\psi=1$ are used in the model proposed in this study, as shown in Equation 12:

$$\frac{\sigma_1}{\sigma_{1max}} = \frac{1}{\sqrt{1 + \left(\xi \cdot \frac{1}{r}\right) + \left(\xi \cdot \frac{1}{r}\right)^2 \beta^2}} \tag{12}$$

2.3.4. Transverse strength of unidirectional composites

As discussed before, the value β depends on the transverse compressive strength σ_{2max} of the composite. In general, only the longitudinal mechanical properties of a composite are of interest for the design of reinforced concrete structures, and therefore the transverse properties of FRP reinforcement are rarely reported by FRP bar manufacturers. A possible way to determine σ_{2max} is by means of compressive tests (as discussed later in section 3.1). Alternatively, if the physical and chemical properties of the composite are known, the transverse properties of a composite can be determined using micromechanical principles. In this way, σ_{2max} can be expressed using Equation 13 as a function of the compressive strength of the resin matrix f_{mc}, a stress concentration factor k_σ, and a residual radial stress at the matrix/fibre interface σ_{rm}. Evaluation of σ_{2max} based on this approach would require, however, the determination of micromechanical properties that are not usually available to designers (Greszczuk 1966).

$$\sigma_{2max} = \frac{1}{k_\sigma}(f_{mc} + \sigma_{rm}) \tag{13}$$

The value k_σ depends on the relative properties of the FRP constituents and on their volume fraction, as shown in Equation 14:

$$k_\sigma = \frac{1 - V_f(1 - E_m/E_f)}{1 - (4V_f/\pi)^{1/2}(1 - E_m/E_f)} \tag{14}$$

where V_f is the fibre volume fraction, E_f is the elastic modulus of the fibres, and E_m is the elastic modulus of the resin matrix.

3. Model verification and design recommendations

3.1. *Experimental programme*

The accuracy of the proposed model at predicting the bend capacity of FRP bars is verified using tests carried out by the authors (Imjai et al. 2017). The test programme included a total of 47 pullout specimens and 19 geometry configurations. Two different types of composite bars were examined: thermoplastic Glass FRP (GFRP) strips (TP), and thermoset GFRP rods (TS), as shown in Figure 7a. The TP specimens were 10 mm wide and 3 mm thick strips and consisted of a thermoplastic polypropylene matrix and continuous unidirectional glass fibres. The strips were bent by applying heat and moulding them around a specially designed device to allow for the fabrication of the required bend radius to thickness ratios. Two different TS circular bars with a diameter of 9.5 mm and 13.5 mm were also investigated. These bars were pre-bent by the manufacturer and had an internal bending radius of 54 mm. Table 1 summarises the main properties of the strip and bars used in the tests by Imjai et al. 2017.

The strips/bars were cast in cubic pullout specimens (types P2 and P3 in Figure 7b) of 200 mm on each side. An unbonded length of 60 mm was used in specimens P2, whilst the full vertical leg of the strips/bars was unbonded in specimens P3. A minimum unbonded length of 60 mm was chosen to minimise the effect of concrete surface cracking on the development of bond stresses during pullout. Full details of the geometry and test data are available in Imjai et al. (2017).

Figures 7c-d compare the results from the pullout tests and the bend capacity of the FRP strips/bars predicted by Equation 12. The comparison is presented as a ratio of average failure stress to ultimate strength in the straight section ($\sigma_{1,avg}/\sigma_{1,max}$). The transverse compressive strength, σ_{2max}, used in this analysis was determined from tests on three 10 mm cube specimens subjected to compressive load in the direction perpendicular to the fibres' axis. Accordingly, the average values σ_{2max} were 96 MPa (Std Dev=0.90 MPa) and 83 MPa (Std Dev=2.8 MPa) for TP

and TS, respectively. The results show that the proposed model (Equation 12) captures well the variation of the bend capacity for different bending radius to bar diameter ratios. It is also shown that the capacity predicted by the proposed model slightly overestimated the test results of specimens P3 (unbonded). This shows that the bond stress along the straight part of the bar plays an important role on the maximum force that is transferred through the bar along the bent and tail region. It should be mentioned that the main objective of testing P3 samples was to examine the capacity of unbonded specimens, which would always give a more conservative bend capacity (regardless the effect of bond between concrete and FRP bar). Overall, the predictions according to the macromechanical model provide in general a lower bound solution, particularly for bonded P2 specimens. The comparisons in Figures 7c-d also indicated that the current equation included in the JSCE guidelines (i.e. Equation 3) tends to overestimate the bend capacity of FRP bars.

3.2.   *Model verification and calibration of β value*

To assess the predictions of the proposed model against real experiments, a total of 80 test data from the literature and tests by the authors were compiled in Table 1. The results are grouped in different datasets, and include the geometry of the bent FRP bars used the tests. All of the specimens in this table were either bent FRP reinforcement embedded in concrete and tested in direct pullout, or tested using a push-off arrangement according to test method B.5 in ACI 440.K (2004). It is also found that the B.5 test method underestimates the bend capacity due to unavoidable eccentricities during the tests, as also reported by Lee et al. (2014).

Table 1 compares the test results $\sigma_{b,avg}$ from the 80 tests with the bend capacity predicted by Equations 1, 2, 3, 4 and the proposed model Equation 12. It should be noted that the parameters needed to determine the value of β were not available for all the specimens listed in Table 1. As mentioned before, the mechanical properties of the constituent materials are rarely given by FRP manufacturers, and therefore the value of β cannot be easily calculated beforehand (note however that β could be inferred using the declared tensile strength, which is usually provided by manufacturers, and other known mechanical properties of the composite). To bypass

this issue, the sensitivity of the model to changes in β was carried out to propose a suitable value of β for practical calculations. Two values of β are shown in Figure 8:

a) β_{set}, which was calculated for each individual dataset so as to yield a mean value of Prediction to Experiment (P/E) capacity ratio of 1 and a minimum standard deviation (SD) for each dataset; and

b) β_{opt}=7.5, which was determined so as to optimise the performance of the proposed model across all the datasets (i.e. P/E=1, SD=min).

The results in Table 1 indicate that the empirical models of Equations 1 to 4 do not predict well the test results and are characterised by high values of standard deviation. For instance, Equation 1 has a P/E=1.66 and a high SD=0.46. The equation developed by JSCE with a value of α=0.05, though still empirical, yields reasonable safer predictions with a P/E=1.02 and a SD=0.27. It is also evident that Equation 12 predicts better the test results (P/E=0.98 and SD=0.18) when different values of β_{set} are used for the different datasets so as to reflect the different type of composites.

Table 1 also shows that the values of transverse strength (σ_{2max}) in datasets 6-7 (JSCE 1997) and 10-11 (Shehata et al. 2000) calculated using the optimised β_{set} factor are higher than the typical values associated with similar types of fibres/matrix combinations (between 90 to 300 MPa). This can be attributed to the fact that the failure criteria implemented in the proposed model is valid for unidirectional composites, while the specimens in these datasets are made of braided or twisted-strand CFRPs, the transverse mechanical properties of which cannot be accurately estimated without further details. On the basis of these considerations, these data were removed from the calibration set prior to determining the optimum value of β_{opt} and a better performance was achieved. In addition, as shown in Figure 8, when using the calculated optimum value of β =7.5, the estimated σ_{2max} ranged from 80-246 MPa, which lies within the typical range for FRP reinforcing composites reported in literature (Hollaway 1993). Figures 9a-b show the performance of Equation 12 as a function of r/d both with and without the datasets 6,7,10 and 11, compared to the equation included in the current design recommendations (Equation 3). The results show that

the proposed model leads to more consistent P/E ratios when β =7.5 for typical recommended values of *r*/*d* below 3-4. Accordingly, if no information about the traversal compressive strength of FRP is available (which is usually the case), it is recommended to use β_{opt} in the calculations. Such value can be then used in Equation 12 for the practical calculation of the bend capacity of FRP bars/strips.

It should be noted that the proposed model ignores bond ('bond factor') between the FRP and concrete. Recent research (Imjai et al. 2017) suggests that the bond characteristics can influence the development of stresses along the embedded portion of the composite. As such, further research and Finite Analyses are currently underway to assess the influence of bond on the results. It is should be also noted that none of the existing models (including Equation 12) account for the influence of concrete strength, embedment length and tail length. These parameters can affect the behaviour of bent bars embedded in concrete and could be responsible for the large variation observed in the test data. In addition, the micromechanical properties of the composites, as well as their constituent materials, should be made available to designers so as to assess the accuracy of bend capacity models in a more rigorous manner.

4. Conclusions

This article proposes a new and practical macromechanical model to predict the bend capacity of FRP bars and strips. The model is based on the Tsai-Hill failure criteria and force equilibrium at the bent zone. The proposed model is calibrated using 25 bent test data carried out by the authors, and then further verified and calibrated against 55 test data from the literature.

The results in this study show that existing predictive models for the capacity of bent bars are mostly derivatives of the Japan Society of Civil Engineers' (JSCE) approach that relies primarily on the bending radius. Such models were found to overestimate the bend capacity of test data from the literature and from the authors, with Prediction/Experiment (P/E) ratios and standard deviations (SD) of up to 1.66 and 0.46, respectively. It is shown that the capacity of bent specimens does not vary only with the r/d ratio, as defined in JSCE based equation. Based on validation and verification of equations from literature, suitable values for the model proposed in

this study are recommended for design. The main parameters considered in the new model include the bending radius to diameter ratio (r/d), a strength factor (β =7.5), a conservative bond factor (φ=0), and a simplified section factor (ψ=1). The proposed model predicts the experimental dataset results more accurately (P/E=1.0) and with less scatter (SD=0.25) compared to predictions given by existing models. The proposed model also to lead to more economic designs by up to 15%.

References

ACI (2004) ACI 440.3R-04 Guide test methods for fiber reinforced polymers (FRPs) for reinforcing or strengthening concrete structures. American Concrete Institute, Farmington Hills, MI, USA.

Ahmed EA, El-Salakawy E, Benmokrane B (2010) Bend strength of FRP stirrups: comparison and evaluation of testing methods. Journal of Composites for Construction, 14(1): 3-10.

BSI (2000) Specification for scheduling, dimensioning, bending, and cutting of steel reinforcement for concrete. British Standard Institution, London, UK.

Ehsani MR, Saadatmanesh H, Tao S (1995) Bond of hooked glass fiber reinforced plastic (GFRP) reinforcing bars to concrete. ACI Materials Journal, 92(4): 391-400.

Gibson RF (1994) Principles of composites material mechanics. McGraw-Hill, New York, USA.

Greszczuk LB (1966) Theoretical and experimental studies on properties and behaviour of filamentary composites. In: Proc. of the Society of Plastic Industry, 21st Annual Conference, Washington, DC, USA.

Hollaway L (1993) Polymer composites for civil and structural engineering. Blackie Academic & Professional, Glasgow, UK.

Imjai T, Guadagnini M and Pilakoutas, K (2009) Curved FRP as concrete reinforcement. Proceedings of the Institution of Civil Engineers - Engineering and Computational Mechanics, 162(3):171-178.

Imjai T, Guadagnini M, Garcia R and Pilakoutas K (2016) A practical method for determining shear crack induced deformation in FRP RC beams. Engineering Structures, 126(1 November 2016), 353-364.

Imjai T, Guadagnini M and Pilakoutas K (2017) Bend Strength of FRP Bars: Experimental investigation and Bond Modelling. Journal of Materials in Civil Engineering, 29(7): 04017024.

Ishihara K, Obara T, Sato Y, Kakuta Y (1997) Evaluation of Ultimate Strength of FRP Rods at Bent-up Portion. In: Proc. of the 3rd International Symposium on Non-Metallic (FRP) Reinforcement for Concrete Structures, Sapporo, Japan, pp 27-34.

Japanese Society of Civil Engineers (1997) Recommendation for design and construction of concrete structures using continuous fiber reinforcing materials. JSCE, Tokyo, Japan.

Lee C, Ko M, Lee Y (2014) Bend strength of complete closed-type carbon fiber-reinforced polymer stirrups with rectangular section. Journal of Composites for Construction, 18(1): 04013022.

Maruyama T, Honama M, Okmura H (1993) Experimental study on tensile strength of bent portion of FRP rods. ACI Special Publication 138, American Concrete Institute, Farmington Hills, MI, pp. 163–176.

Maruyama T, Honma M, Okamura H (1995) Experimental Study on Tensile Strength of Bent Portion of FRP Rods. In: Proc. of 2nd RILEM symposium (FRPRCS-2), Ghent, Belgium, pp 163-176.

Miyata S, Tottori S, Terada T, Sekijima K (1989) Experimental study on tensile strength of FRP bent bar. Transactions of The Japanese Concrete Institute, 11, pp.185-191.

Nakamura H, Higai I (1995) Evaluation of shear strength on concrete beams reinforced with FRP. Concrete Library, Japanese Society of Civil Engineers, 26, pp 111-123.

Nagasaka T, Fukuyama H, Tanigaki M (1989) Shear Performance of Concrete Beam Reinforced with FRP Stirrups. Transactions of The Japanese Concrete Institute, 11:789-811.

Pilakoutas K, Guadagnini M, Neocleous K, Matthys S (2011) Design guidelines for FRP reinforced concrete structures. Proceedings of the Institution of Civil Engineers - Structures and Buildings, 164(4): 255-63.

Shehata E, Morphy R, Rizkalla S (2000) Fiber reinforced polymer shear reinforcement for concrete members: Behavior and design guidelines. Canadian Journal of Civil Engineering, 27:859–872.

Stuart V, Cunningham LS (2017) FRP reinforced-concrete slabs: a comparative design study. Proceedings of the Institution of Civil Engineers - Structures and Buildings, 170(8): 581-602.

Tsai SW, Hahn HT (1980) Introduction to Composite Materials. Technomic Publishing Company Inc, Lancaster, PA, USA.

Ueda T, Sato Y, Kakuta Y, Imamura A, Kanematsu H (1995) Failure criteria for FRP rods subjected to a combination of tensile and shear forces. In: Proc. of 2nd RILEM symposium (FRPRCS-2), Ghent, Belgium, pp 26-33.

Weatherhead R (1980) FRP Technology: Fibre Reinforced Resin Systems. Applied Science Publishers Ltd, London, UK.
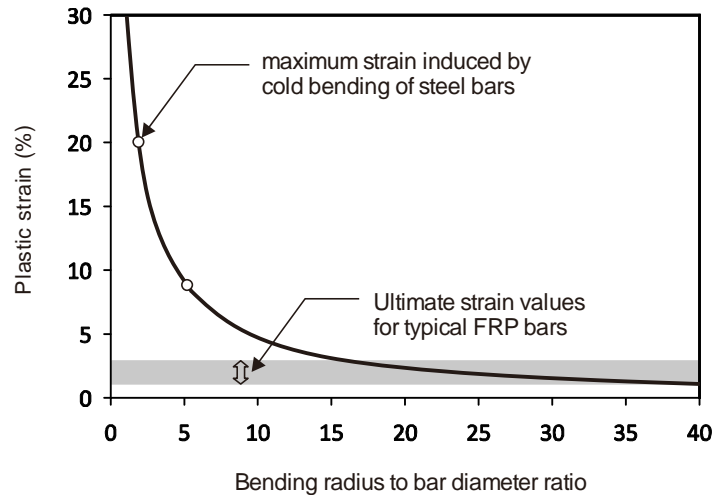
Figure 1 Strain induced in cold bent bars
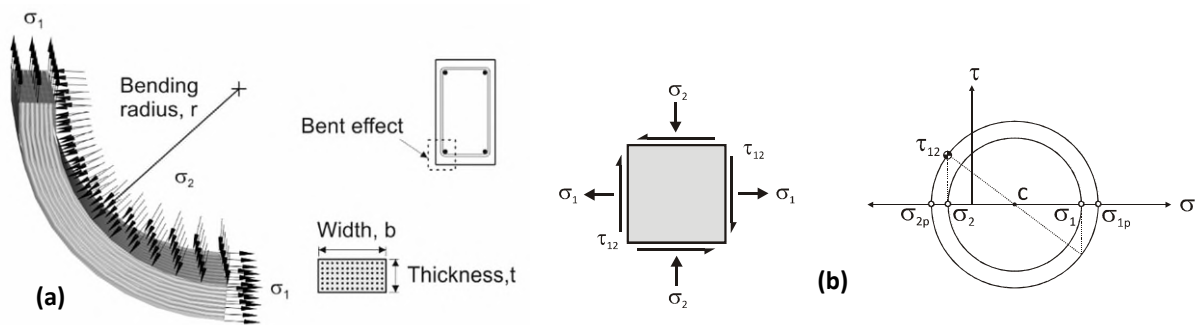
Figure 2 (a) Average stresses acting on a rectangular bent bar embedded in concrete, and (b)

bond stress on the principal stresses on Mohr's circle
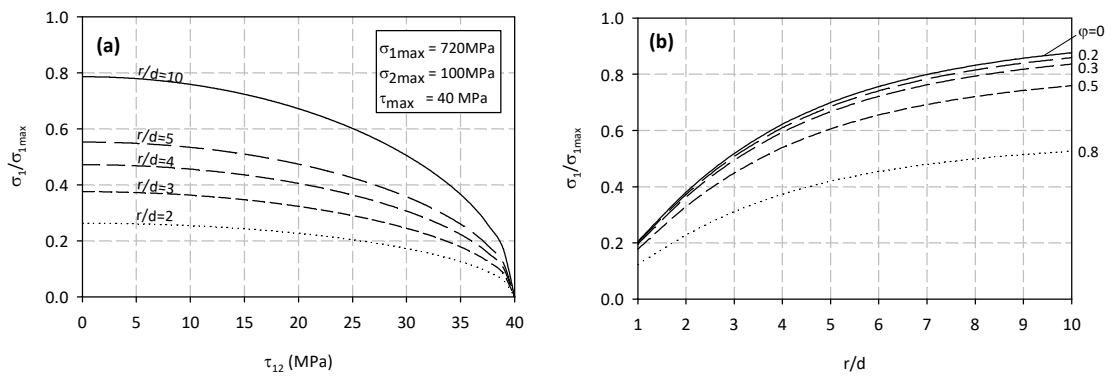
Figure 3 Effect of (a) shear stress, and (b) bond factor φ on the bend capacity of a FRP bar
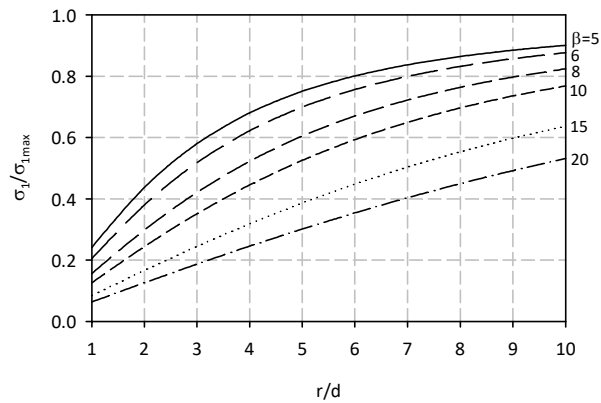
Figure 4 Effect of the strength factor β on the bend capacity of a FRP bar
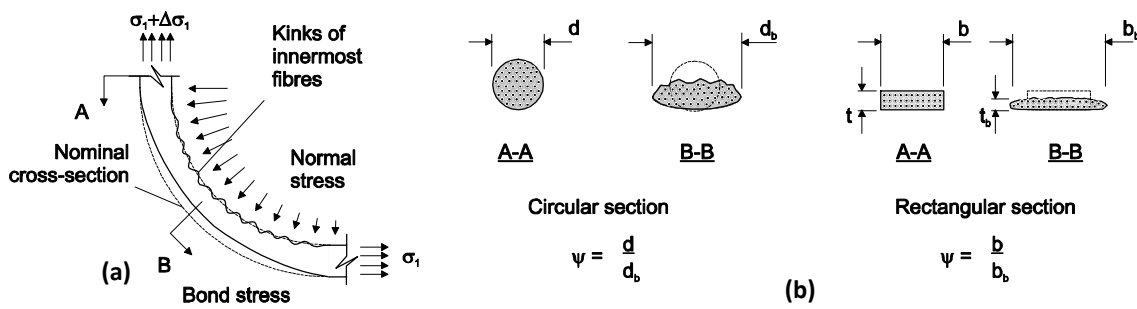
Figure 5 (a) Premature failure at the innermost fibre of FRP bars, and (b) section factor ψ as a

function of cross-section variations
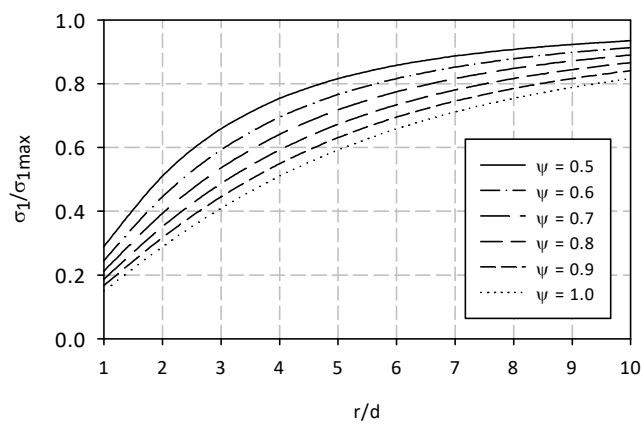
Figure 6 Effect of the shape factor ψ on the bend capacity of a FRP bar

18
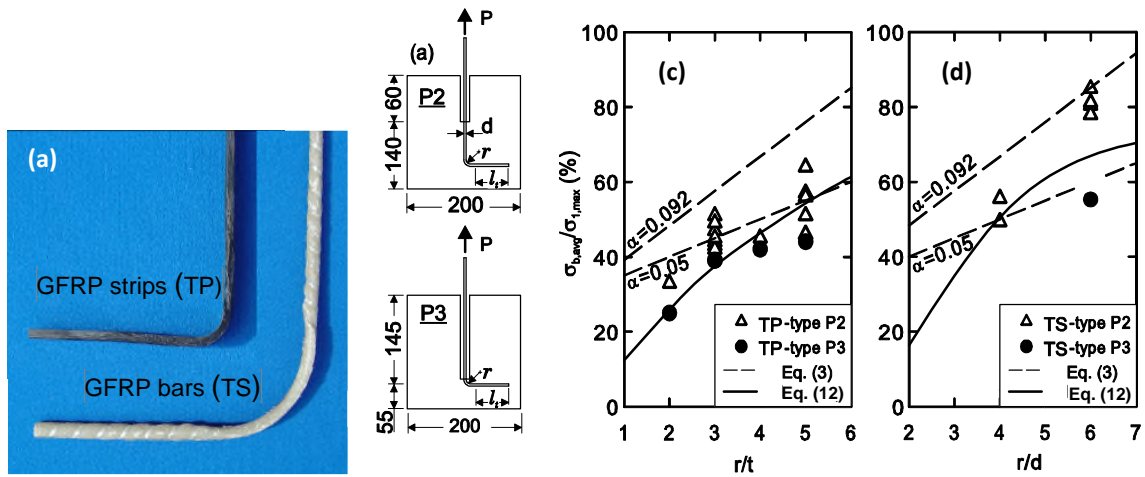
Figure 7 (a) GFRP strips (TP) and rods (TS), (b) pullout specimens tested by Imjai et al. (2017), and (c) test results vs predictions of bend capacity calculated with proposed model (Equation 12) and JSCE equation.
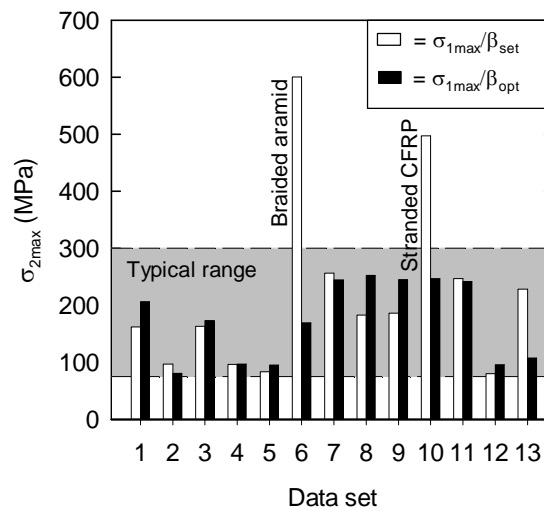
Figure 8 Comparison of calculated transverse strength of composites according to different values of β (refer to dataset number in Table 2)
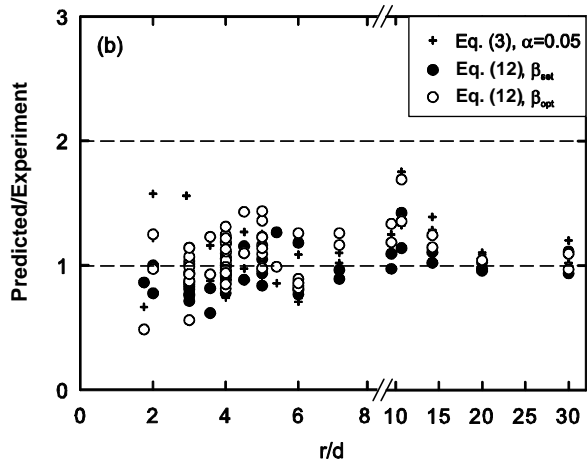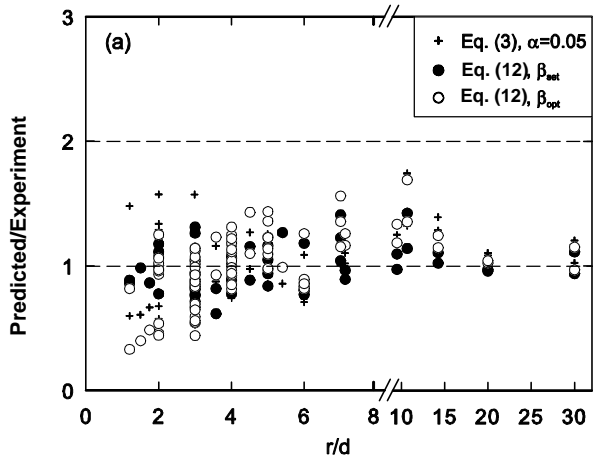
Figure 9 Performance of the proposed model as a function of r/d, (a) with and (b) without datasets 6,7,10 and 11

Table 1 Properties of the strip and bars used in the tests by Imjai et al. 2017

Property	TP strip	TS bar 9.5 mm	TS bar 13.5 mm
Size (mm)	10×3	9.5	13.5
Tensile strength (MPa)	720	760	690
Tensile modulus (GPa)	28	40.8	40.8
Ultimate strain (%)	1.9	1.1	1.1
Glass content (% v/v)	35	70	70

Table 2 Comparison of bend capacity of FRP bars/strips predicted by different models and test results

Reference	ID	Composite type [dataset number]	d (mm)	r (mm)	d_{fi} (mm)	r/d	r/d_{fi}	l_b/d	l_t/d	σ_{1max} (MPa)	$\sigma_{b,avg}$ (MPa)	Eq. 1	Eq. 2	Eq. 3		Eq. 4	Eq. 12	
														$\alpha=0.05$	$\alpha=0.092$		β_{set}	β_{opt}
(a) Imjai et al. (2017)	1	GFRP strip [1]	3	6	3.39	2.0	1.8	46	10	720	236	584	442	288	348	364	227	244
	2		3	9	3.39	3.0	2.7	46	10	720	309	621	485	324	415	377	318	339
	3		3	12	3.39	4.0	3.5	47	10	720	324	643	514	360	481	389	393	414
	4		3	15	3.39	5.0	4.4	48	10	720	370	656	536	396	547	402	451	472
	5		3	9	3.39	3.0	2.7	46	10	720	316	621	485	324	415	377	318	339
	6		3	15	3.39	5.0	4.4	48	10	720	415	656	536	396	547	402	451	472
	7		3	9	3.39	3.0	2.7	46	10	720	340	621	485	324	415	377	318	339
	8		3	15	3.39	5.0	4.4	48	10	720	399	656	536	396	547	402	451	472
	9		3	9	3.39	3.0	2.7	46	10	720	367	621	485	324	415	377	318	339
	10		3	15	3.39	5.0	4.4	48	10	720	464	656	536	396	547	402	451	472
	11		3	9	3.39	3.0	2.7	41	5	720	299	621	485	324	415	377	318	339
	12		3	15	3.39	5.0	4.4	43	5	720	334	656	536	396	547	402	451	472
	13		3	9	3.39	3.0	2.7	48	12	720	324	621	485	324	415	377	318	339
	14		3	9	3.39	3.0	2.7	51	15	720	345	621	485	324	415	377	318	339
	15		3	6	3.39	2.0	1.8	14	10	720	183	584	442	288	348	364	227	244
	16		3	9	3.39	3.0	2.7	15	10	720	280	621	485	324	415	377	318	339
	17		3	12	3.39	4.0	3.5	17	10	720	301	643	514	360	481	389	393	414
	18		3	15	3.39	5.0	4.4	19	10	720	316	656	536	396	547	402	451	472
	19		3	9	3.39	3.0	2.7	15	10	720	281	621	485	324	415	377	318	339
	20	GFRP Rod [2]	9	54	9	6.0	6.0	20	5	760	611	703	583	456	648	448	494	545
	21		9	54	9	6.0	6.0	22	7	760	645	703	583	456	648	448	494	545
	22		9	54	9	6.0	6.0	20	5	760	592	703	583	456	648	448	494	545
	23		9	54	9	6.0	6.0	22	7	760	617	703	583	456	648	448	494	545
	24		13.5	54	13.5	4.0	4.0	15	5	590	382	527	422	295	394	325	296	339
	25		13.5	54	13.5	4.0	4.0	15	5	590	345	527	422	295	394	325	296	339
	26		9	54	9	6.0	6.0	20	5	760	419	703	583	456	648	448	494	545
(b) Ahmed et al. (2010)	27	CFRP Rod [3]	9.5	38	9.50	4.0	4.0	11	6	1538	712	1373	1099	769	1027	846	712	883
	28	GFRP Rod [4]	9.5	38	9.50	4.0	4.0	11	6	664	387	593	474	332	444	365	407	381
	29		15.9	63.6	15.90	4.0	4.0	11	6	599	404	535	428	300	400	329	367	344
	30		19.1	76.4	19.10	4.0	4.0	11	6	533	310	476	381	267	356	293	327	292

Ref.	ID	Composite types	d (mm)	r (mm)	d_{fi} (mm)	r/d	r/d_{fi}	l_b/d	l_t/d	σ_{lmax} (MPa)	$\sigma_{b,avg}$ (MPa)	Eq. 1	Eq. 2	Eq. 3 $\alpha=0.05$	Eq. 3 $\alpha=0.092$	Eq. 4	Eq. 12 β_{set}	Eq. 12 β_{opt}
(c) El-Sayed et al. (2007)	31	CFRP rod [5]	9.5	38.1	9.50	4.0	4.0	5	6	1328	701	1186	949	665	888	731	698	764
	32		9.5	38.1	9.50	4.0	4.0	5	9	1328	761	1186	949	665	888	731	698	764
	33		9.5	38.1	9.50	4.0	4.0	5	12	1328	656	1186	949	665	888	731	698	764
	34		9.5	38.1	9.50	4.0	4.0	5	15	1328	596	1186	949	665	888	731	698	764
	35		9.5	38.1	9.50	4.0	4.0	5	20	1328	789	1186	949	665	888	731	698	764
	36		12.7	50.8	12.70	4.0	4.0	5	3	1224	681	1093	874	612	818	673	643	703
	37		12.7	50.8	12.70	4.0	4.0	5	6	1224	539	1093	874	612	818	673	643	703
	38		12.7	50.8	12.70	4.0	4.0	5	9	1224	697	1093	874	612	818	673	643	703
(d) JSCE (1997)	39	Braided AFRP rod with epoxy [6]	8	16	8	2.0	2.0	N/A	N/A	1369	812	1110	840	548	663	698	952	463
	40		6	12	6	2.0	2.0	N/A	N/A	1142	796	926	700	457	553	582	794	387
	41		8	12	8	1.5	1.5	N/A	N/A	1369	846	1049	778	513	600	685	830	359
	42		10	12	10	1.2	1.2	N/A	N/A	1283	775	933	684	462	527	634	683	273
	43		6	12	6	2.0	2.0	N/A	N/A	1142	824	926	700	457	553	582	794	387
	44	7-stranded CFRP rod with epoxy [7]	8	16	8	2.0	2.0	N/A	N/A	1794	557	1455	1100	718	868	915	596	607
	45		6	12	6	2.0	2.0	N/A	N/A	1620	552	1314	994	648	784	826	538	548
	46		8	16	8	2.0	2.0	N/A	N/A	1794	595	1455	1100	718	868	915	596	607
	47		10	12	10	1.2	1.2	N/A	N/A	2271	553	1652	1211	818	932	1122	474	484
	48		6	12	6	2.0	2.0	N/A	N/A	1620	485	1314	994	648	784	826	538	548
(e) Lee et al. (2014)	49	CFRP rod [8]	9.5	42.8	9.50	4.5	4.5	28	19	1880	778	1698	1373	987	1343	1053	896	1161
	50		9.5	42.8	9.50	4.5	4.5	28	19	1880	1014	1698	1373	987	1343	1053	896	1161
	51	CFRP strip [9]	4	14.3	4.51	3.6	3.2	68	60	1850	763	1631	1293	886	1163	987	762	987
	52		4	14.3	4.51	3.6	3.2	68	60	1850	1012	1631	1293	886	1163	987	762	987
	53		4	28.5	4.51	7.1	6.3	68	53	1850	1102	1731	1456	1214	1768	1103	1224	1424
	54		4	28.5	4.51	7.1	6.3	68	53	1850	1192	1731	1456	1214	1768	1103	1224	1424
	55		4	42.8	4.51	10.7	9.5	68	46	1850	935	1769	1535	1545	1850	1220	1465	1604
	56		4	42.8	4.51	10.7	9.5	68	46	1850	1167	1769	1535	1545	1850	1220	1465	1604
	57		3	28.5	3.39	9.5	8.4	90	71	1740	1079	1654	1423	1349	1740	1111	1318	1466
	58		3	28.5	3.39	9.5	8.4	90	71	1740	1215	1654	1423	1349	1740	1111	1318	1466
	59		3	42.8	3.39	14.3	12.6	90	61	1740	1267	1682	1490	1763	1740	1258	1499	1589
	60		3	42.8	3.39	14.3	12.6	90	61	1740	1373	1682	1490	1763	1740	1258	1499	1589
	61		0.9	18	1.02	20.0	17.7	300	260	1880	1731	1835	1660	1880	1880	1550	1724	1782
	62		0.9	18	1.02	20.0	17.7	300	260	1880	1703	1835	1660	1880	1880	1550	1724	1782
	63		0.9	27	1.02	30.0	26.6	300	240	1880	1882	1849	1710	1880	1880	1880	1799	1827
	64		0.9	27	1.02	30.0	26.6	300	240	1880	1586	1849	1710	1880	1880	1880	1799	1827

Ref.	ID	Composite types	d (mm)	r (mm)	d_{fi} (mm)	r/d	r/d_{fi}	l_b/d	l_t/d	σ_{1max} (MPa)	$\sigma_{b,avg}$ (MPa)	Eq. 1	Eq. 2	Eq. 3 α =0.05	Eq. 3 α =0.092	Eq. 4	Eq. 12 β_{set}	Eq. 12 β_{opt}
(f) Shehata et al. (2000)	65	7-stranded CFRP pre-stressing cable (CFCC) [10]	3.59	10.8	3.59	3.0	3.0	4	N/A	1782	916	1538	1201	802	1026	944	1199	838
	66		3.59	10.8	3.59	3.0	3.0	4	N/A	1782	1455	1538	1201	802	1026	944	1199	838
	67		4.4	13.2	4.40	3.0	3.0	4	N/A	1842	983	1590	1241	829	1061	976	1239	866
	68		4.4	13.2	4.40	3.0	3.0	4	N/A	1842	1187	1590	1241	829	1061	976	1239	866
	69		6.22	18.7	6.22	3.0	3.0	24	N/A	1875	1900	1618	1264	844	1080	994	1261	882
	70		6.22	18.7	6.22	3.0	3.0	12	N/A	1875	1421	1618	1264	844	1080	994	1261	882
	71		6.22	18.7	6.22	3.0	3.0	4	N/A	1875	798	1618	1264	844	1080	994	1261	882
	72	CFRP strip (Leadline) [11]	5	15.0	5.00	3.0	3.0	30	N/A	1800	1242	1553	1213	810	1037	954	815	846
	73		5	15.0	5.00	3.0	3.0	4	N/A	1800	715	1553	1213	810	1037	954	815	846
	74		5	35.0	5.00	7.0	7.0	30	N/A	1800	1163	1682	1413	1170	1699	1098	1350	1376
	75		5	35.0	5.00	7.0	7.0	12	N/A	1800	988	1682	1413	1170	1699	1098	1350	1376
	76		5	35.0	5.00	7.0	7.0	8	N/A	1800	858	1682	1413	1170	1699	1098	1350	1376
	77	C-Bar GFRP [12]	12	48.0	12.00	4.0	4.0	5	N/A	713	346	636	509	357	476	392	346	410
(g) Vint and Sheikh (2014)	78	GFRP rod [13]	9.43	51	9.43	5.4	5.4	5	33.09	833	555	764	628	475	664	481	701	568
	79		11.93	36	11.93	3.0	3.0	5	26.15	655	522	565	441	295	377	347	450	308
	80		13	23	13	1.8	1.8	5	24	912	531	721	540	353	420	461	457	275
Mean value (Prediction / Experiment)												*1.66*	*1.34*	*1.02*	*1.28*	*1.08*	*0.98*	*1.00*
Standard deviation (Prediction / Experiment)												*0.46*	*0.33*	*0.27*	*0.32*	*0.28*	*0.18*	*0.25*

Note: r is the internal bending radius, d is the nominal diameter (diameter for circular section and thickness for strip), d_{fi} is the transformed diameter, l_b is the total bonded length that embedded in a concrete cube, l_t is the tail length measured after the bend, $\sigma_{b,avg}$ is the experimental average failure stress, and σ_{1max} is the ultimate strength of the FRP bar.